Investigation of the utility of complementary electrochemical detection techniques to examine the in vitro affinity of bacterial flagellins for a toll-like receptor 5 biosensor

Zhe She[12‡], Kristin Topping[3‡], Mohtashim H. Shamsi[24], Nan Wang[12†], Nora W.C. Chan[35], and Heinz-Bernhard Kraatz*[123]

[1]Department of Physical and Environmental Sciences, University of Toronto Scarborough, 1265 Military Trail, Toronto, ON, M1C 1A4, Canada. [2]Department of Chemistry, 80. St. George Street, Toronto, M5S 3H6, Canada. [3]Department of Chemistry and Chemical Engineering, Royal Military College of Canada, PO Box 17000, Station Forces, Kingston, ON, K7K 7B4,Canada. [4]Donnelly Centre for Cellular and Biomolecular Research, 160 College Street, Toronto, ON, M5S 3E1, Canada. [5]Bio-Analysis Group, Defence Research and Development Canada – Suffield Research Centre, P.O. Box 4000, Station Main, Medicine Hat, Alberta, T1A 8K6, Canada.

ABSTRACT: An initial investigation of the fabrication of a novel biosensor utilizing toll-like receptor 5 (TLR5) has been conducted. The detection assay using this sensor platform has been carried out using four complementary electrochemical techniques. The electrochemical properties of the modified bare gold surface following TLR5 immobilization were characterized. The electrochemical response to changes in the sensor film resistance and electron charge transfer permittivity triggered by independent exposures to flagellins from *Salmonella typhimurium (S. typhim.)* and *Bacillus subtilis (B. subtilis)* were examined and observed. The quantified film resistance data gathered using electrochemical impedance spectroscopy (EIS) over a macroscopic scale are in significant agreement with the corresponding electron charge transfer permittivity measured locally by scanning electrochemical microscopy (SECM). Unlike other sensors that exploit pathogen recognition elements, TLR5 biosensors have the potential to carry out broad-spectrum detection of flagellated bacterial pathogens in near-real time. This broad-spectrum detection platform is a significant step towards the development of fast, inexpensive clinical tools for early warning diagnoses and immediate on-site treatment.

Introduction

Bacterial whole cell detection using bio-recognition element sensors has been examined using a variety of analytical detection techniques such as: reflectometric interference spectroscopy[1], fluorescence,[2] quartz crystal microbalance,[3,4] electrochemistry[5-7] and surface plasmon resonance (SPR).[8,9] Specific recognition of bacteria via electrochemical methods has been carried out using specially fabricated electrodes with immobilized bio-recognition elements. In this context, effective detection of *E. coli* O157:H7 has been reported.[10,11] These experiments exploited a sensor architecture that included the attachment of a ferrocene-receptor peptide conjugate onto a gold surface, followed by the interaction of *E. coli* with the peptide component of the conjugate, Magainin-I, an antimicrobial peptide. While this is a good example of electrochemical detection of one particular strain of bacteria, there is still an urgent need to detect broad-spectrum bacterial agents. In a real world scenario, real-time, strain-specific identification of a bacterial pathogen is not practical. Instead, an early warning, broad-spectrum classification method could be very useful for early treatment following exposure to a bacterial strain. The broad-spectrum nature of this type of sensor is also advantageous because it does not preclude the detection of novel bacterial agents.

In more recent studies, focus has been on analyzing the efficacy of sensors designed to recognize specific bacterial chemical markers, referred to as pathogen-associated molecular patterns (PAMPs), rather than on whole cell detection.[12-14] These markers include, but are not limited to, intercellular entities such as DNA[8,15-23] or extracellular components such as LPS[24-27]. One class of bio-recognition elements, which are particularly appealing for broad-spectrum bacterial detection via PAMP interaction, is the toll-like receptors (TLRs). The TLRs are a vital component of the innate immune response. These type I transmembrane glycoproteins are expressed by a variety of immune and non-immune cells, such as dendritic cells, macrophages, B-cells and epithelial cells.[28,29] *In vivo*, the suite of TLRs are used to detect the invasion of antigens and are specifically triggered by the conserved PAMPs of Gram-negative (-) or Gram-positive (+) bacteria, viruses or fungi.[30] Each TLR specifically interacts with a different cell wall or nucleic acid PAMP.[31] Toll-like receptors have shown to be powerful broad-spectrum bio-recognition elements, used as early-warning indicators for the invasion of pathogenic moieties.[32]

Optical detection methods, such as SPR have been exploited for pathogen detection using TLR sensor surfaces.[24,32] In this study, we focus on toll-like receptor 5 (TLR5) which

selectively binds to Gram-negative and Gram-positive bacterial flagellins.[32,33] Sensors exploiting TLR5 as the bio-recognition element with electrochemical detection are a novel approach toward the detection of motile bacteria. The combined strategy of applying electrochemical detection methods and TLR recognition elements offers several incremental advantages over detection by optical analytical techniques. These advantages include a reduction in the overall amount of materials required for immobilization and the cumulative production of less effluent/waste.[7,32,34] Electrochemical potentiostats also have smaller power requirements than SPR equipment, therefore commercial-off-the-shelf, hand-held systems are available for portable, on-site detection.[34]

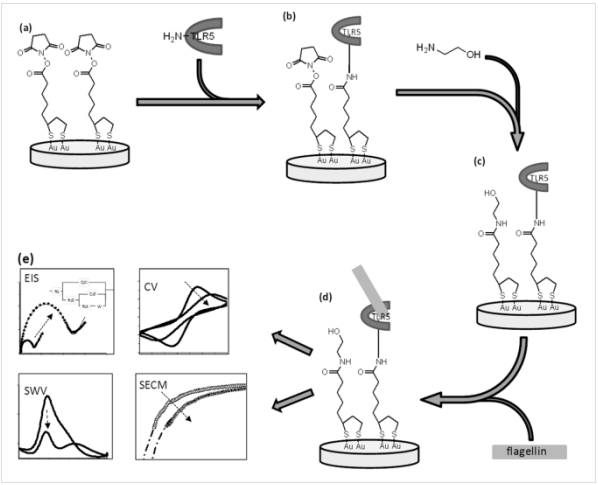

Figure 1. Schematic depicting the production of the TLR5 biosensor architecture followed by the electrochemical detection of flagellins. (a) Gold modified with lipoic acid n-hydroxysuccinimide ester (LPA); (b) immobilization of TLR5 protein via amine-coupling; (c) blocking the unreacted LPA amine sites with ethanolamine; (d) binding of flagellins with TLR5 protein; (e) The electrochemical signal triggered by binding reaction is monitored by electrochemical impedance spectroscopy, cyclic voltammetry, square-wave voltammetry and SECM respectively.

In this study, we have carried out an initial investigation into the efficacy of using TLR5 as an immobilized bio-recognition element for the detection of its respective PAMPs, Gram-negative and Gram-positive bacterial flagellins. Unique electrochemical responses invoked when, in the flagellins of *S. typhim.* and *B. subtilis*, in independent experiments, bind to the TLR5-receptor have been monitored and examined using several different, yet complementary detection techniques, including electrochemical impedance spectroscopy (EIS), cyclic voltammetry (CV), square-wave voltammetry (SWV) and scanning electrochemical microscopy (SECM). This label-free detection scheme, as illustrated in the Figure 1, may be exploited in the future for the development of sensors for near-real time, broad-spectrum bacterial pathogen diagnostics. While pathogen recognition is not species- or strain-specific, the direct interaction of a class of pathogen ligands, flagellins makes this detection scheme very attractive as a broad-spectrum biosensor.

Experimental Methods

The experimental reagents and processes for electrode cleaning and preparation of TLR5 sensors are described in the supporting information.

Exposure of biosensors to flagellin analytes. Blocked TLR5 biosensors were incubated in either *S. typhim.* (-) flagellins or *B. subtilis* (+) flagellins at various concentrations for 5 minutes and rinsed thoroughly with an excess of water before further characterization by CV, SWV and EIS. Separate TLR5 Gold/Silicon (Au/Si) substrates, blocked with ethanolamine, were incubated in either 2 μM of *S. typhim.* flagellins or 2 μM of *B. subtilis* flagellins respectively for 5 minutes. These substrates were used for SECM measurements.

Electrochemical measurements. All experimental measurements were taken with the electrochemical cell enclosed within a Faraday cage. CV, SWV and EIS measurements were carried out using a CHI-660b potentiostat (CH Instruments, Austin, TX) in an electrochemical cell equipped with a three-electrode configuration. Receptor-modified gold electrodes are the working electrode and platinum (Pt) wire is used for the counter electrode. A reference electrode (Ag/AgCl/3.0 M KCl) and a salt bridge, filled with an agar and 1 M KNO_3 aqueous solution, were inserted to minimize the diffusion of chloride ions into the electrolyte solution. The agar solution was prepared by dissolving 2 grams of agar and 10.1 g KNO_3 in 100 mL of water. The CV, SWV and EIS electrolyte consisted of a 5 mM $K_4Fe(CN)_6$/5 mM $K_3Fe(CN)_6$ aqueous solution with 1 M of $NaClO_4$ as the supporting electrolyte. For consistency, the electrochemical measurements were carried out with open-circuit potentials. EIS experiments were conducted in the frequency range of 100,000 to 0.1 Hz with an amplitude of 5 mV. The experimental EIS curves were evaluated to determine the film resistance using ZSimpWin 2.0 software.

Scanning electrochemical microscopy. SECM experiments were carried out with CHI-900b (CH Instruments, Austin, TX) at room temperature. Modified Au/Si substrates were mounted in an electrochemical cell using a three-electrode configuration. A Pt wire, an Ag/AgCl/3.0 M KCl electrode and a Pt tip were fitted as the counter electrode, reference electrode and working electrode respectively. The SECM electrolyte consisted of 2 mM $K_4Fe(CN)_6$ aqueous solution as the redox probe and 50 mM $NaClO_4$ as the supporting electrolyte. The homemade Pt tip was manufactured by sealing a Pt wire with diameter of 25 μm into a glass capillary. After which, the microelectrode was polished to an RG~5 (ratio of total microelectrode radius to Pt wire radius). The tip was electrochemically cleaned prior to each experiment by running a CV method with this electrode immersed in a 0.5 M H_2SO_4 solution between 0 V and 1.4 V for 100 cycles at a scan rate of 0.5 $V \cdot s^{-1}$. A constant potential of 0.5 V was applied for all approach curve measurements. Upon application of this potential, the steady-state current was obtained by holding the Pt tip, immersed in the electrolyte, at a constant height above the substrate for 300 seconds before commencing the approach. The modified Au/Si substrates were not biased during the measurement. The experimental approach curves were normalized to the steady-state current before fitting them against theoretical curves generated using COMSOL Multiphysics software.[35-37] Subsequently, the reaction kinetics for the modified surfaces was estimated.

Results and Discussions

CV was performed to characterize the electrode surface with and without architectural modifications using a $Fe(CN)_6^{3-/4-}$ probe. The CV scans obtained on unmodified gold electrodes have oxidation and reduction peaks at approximately 0.28 V

and 0.21 V respectively, as depicted by the black lines in Figure S1a. The oxidation peak moves to a slightly more positive potential of 0.30 V after the gold electrode is modified with LPA. The corresponding reduction peak shifts towards a less positive potential of 0.19 V. This observation is logical, as an LPA self-assembled monolayer (SAM) is formed on the gold electrode after this modification step. LPA SAMs are more passive with respect to electron transfer permittivity and therefore require more over-potential for the redox reaction of $Fe(CN)_6^{3-/4-}$. Also observed in the CV data, is an overall reduction in the current density values. This is due to the LPA SAMs blocking most of the surface and, thus, reducing the effectiveness of electron transfer between the gold and the redox probe, $Fe(CN)_6^{3-/4-}$. TLR5 proteins are immobilized onto the intermediate LPA SAM via amine-coupling. In comparison to the LPA molecules (molar mass = 303 $g \cdot mol^{-1}$), TLR5 proteins have a molar mass of 97.3 kD. Consequently, it is expected that the surface charge permittivity would decrease further following the addition of the TLR5 proteins to the sensor architecture. This hypothesis is proved consistent with the experimental CV results. As shown in Figure S1a, both the oxidation and reduction peaks shift outwards and the current densities decrease further as the electrons and redox probe ions have to diffuse through a significantly more hindered environment. CV scans were also obtained after treating the sensor surfaces with ethanolamine blocking solution. Blocking the unreacted LPA amine sites with ethanolamine limits the immobilization of non-TLR5 surface-fouling proteins that are ubiquitous in the environment.[38] The ethanolamine molecule is relatively small therefore there was a small decrease in the peak current density values. The same incremental surface architecture assembly was examined using EIS as shown in the Nyquist plots in Figure S1b. The plots were fitted using the inset model in order to evaluate the film resistance (Rct); the modeled data is shown as continuous lines in Figure S1b. A plot of the evaluated Rct following each modification step, as garnered from repeated measurements, is shown in Figure S1c. The modeled experimental Rct of the LPA layer was determined to be 572 ± 124 ohm$\cdot cm^{-2}$, as shown in Figure S1c, with a 1-sigma error of approximately 20%. The Rct increases to 1580 ± 125 ohm$\cdot cm^{-2}$ following immobilization of TLR5 and the value increased further, but less appreciably, following ethanolamine blocking to 1631 ± 427 ohm$\cdot cm^{-2}$. The change in the electrode surface character following the receptor-ligand interaction can be more clearly visualized using EIS, as compared to the corresponding CV plots.

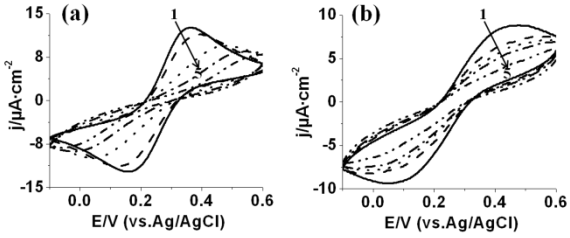

Figure 2. Cyclic voltammogram obtained, first, for the TLR5 sensor before ligand immersion and then after exposure to various concentrations of (a) *S. typhim*., a Gram(-) species and (b) *B. subtilis*, Gram(+). The corresponding concentrations of species are 0 μM (before immersion), 0.1 μM, 0.5 μM, 1 μM and 2 μM from 1 to 5. The scan rate was 0.1 $V \cdot s^{-1}$ and measurements were carried out in a 5 mM/5 mM $Fe(CN)_6^{3-/4-}$ aqueous solution with 1 M $NaClO_4$ as the supporting electrolyte.

In vivo, TLR5 proteins recognize most flagellated bacteria, specific recognition is mediated by interaction with the protein monomer (flagellin) that constitutes the flagella filament[33]. Two flagellin variants extracted from *S. typhim*., a Gram(-) species and *B. subtilis*, Gram(+), are applied to test the efficacy of the sensor. The major difference between these ligands is their respective molecular weights, the Gram(-) flagellins being the heavier of the two at 50 kDa while the Gram(+) flagellins used in these experiments weighs in at 32 kDa. After immersing blocked TLR5 electrodes in each concentration of the ligand solutions for 5 minutes, the CV scans, as shown in Figure 2, show the flatterning of cycle curves and much lower current densities, observation that are consistent with the binding of the flagellin protein polymer onto the immobilized TLR5 and the increased insulation of the thicker surface layer. Correspondingly, it can be seen that the current density decrease is influenced by the increase in concentration of the ligand exposed as shown in Figure 2a and b. When comparing the current density changes following sensor exposure to the same concentration of each of the two ligands independently, the decrease in the measured current density for the *S. typhim.* flagellin application was consistently larger than that measured for the *B. subtilis* flagellin application. Once again this difference can be attributed to the significant difference in the molecular weight between these ligands. Although the CV technique is not readily adapted to a mobile sensor, the speed and ease with which CV curves can be obtained make this detection method ideal for ensuring quality control when carrying out each step in the sensor surface modification procedure. The detection of the ligand species with the modified TLR5 sensor architecture was also examined using SWV.

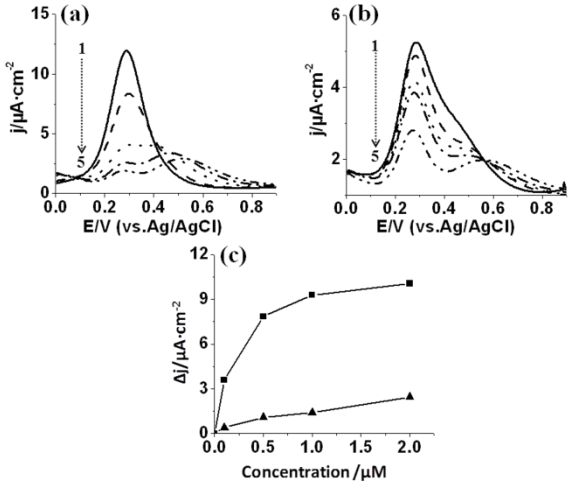

Figure 3. Square-wave voltammogram obtained, first, for the TLR5 sensor before ligand immersion and then after exposure to various concentrations of (a) *S. typhim*., a Gram(-) species and (b) *B. subtilis*, Gram(+). The corresponding concentrations of species are 0 μM (before immersion), 0.1 μM, 0.5 μM, 1 μM and 2 μM from 1 to 5. A plot (c) summarizing the current density change (Δj) upon exposure of the TLR5 sensor platform to various concentration of the respective ligands, *S. typhim*. (■) and *B. subtilis* (▲).

A current peak at 0.3 V was observed when an SWV measurement is taken for a TLR5 sensor prior to immersion in *S. typhim.*, as shown in the Figure 3a. The current peak and corresponding peak area decreases after exposing the sensor to the *S. typhim.* flagellin solutions. The higher the ligand

concentration, the smaller the measured current peak height and peak area. While the current peak at 0.3 V decreases, a broad low current peak rises at 0.5 V for sensors exposed to higher concentrations of *S. typhim*. flagellins. This could imply, that as the total number of available TLR5 receptors on the electrode surface bind to more ligands, due to their increased availability in higher concentration flagellin solutions, the cumulative architecture has a higher packing factor. The higher packing factor results in a blocking effect and, thus, an increased current density at a higher applied potential. This same behavior was also observed for the detection of *B. subtilis* ligands on the TLR5 sensor, as shown in Figure 3b, but the changes in current density is smaller. These SWV results are consistent with the CV measurements previously described. The observed current density changes, between the bare TLR5 sensor and following TLR5-ligand binding reaction are summarized in the plots shown in Figure 3c. This figure visually depicts the comparative change in current density for binding reactions using low *S. typhim.* ligand concentrations as compared to high ones. The resulting curve illustrates a potential saturation of the available TLR5 binding sites on the sensor by the available ligands in solution. An upper limit has been reached in the allowable change in current density based on that level of TLR5 immobilization on the sensor surface. These Langmuir adsorption-like plots have been observed in many other detection scenarios.[9,20,39] In contrast, the plot shows a more linear behavior for the ligand of *B. subtilis*., which has a lower molar mass, for the concentration range explored in this study. This observation, in comparison with the results for the *S. typhim* flagellins, may indicate that TLR5 has a higher binding affinity for Gram(-) flagellins than for those of Gram(+) bacteria. The saturation of the TLR5 sensor surface has not yet been demonstrated for the latter, despite applying the same solution concentration of that ligand. A more in-depth study of the TLR5 interaction with ligands from a wider breadth of bacterial species is required to confirm this hypothesis.

In addition to CV and SWV, EIS is another very powerful technique to be applied for label-free detections.[7,10,40]

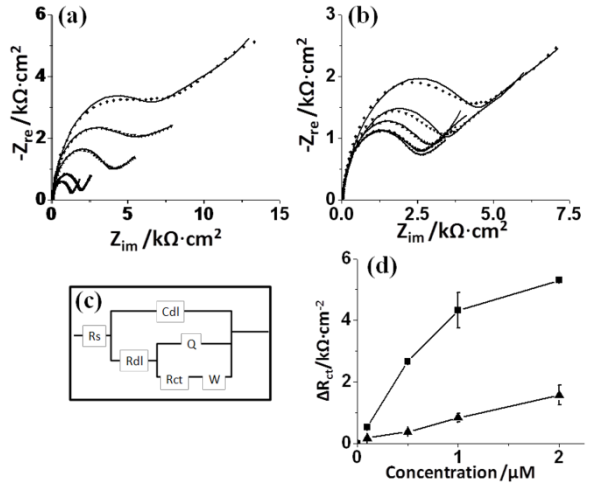

Figure 4. Nyquist plots before and after exposing the TLR5 sensor to ligands of *S. typhim*. (a) and *B. subtilis* (b) at solution concentrations of 0.1 μM, 0.5 μM, 1 μM and 2 μM respectively. Impedance results were recorded from 100 kHz to 0.1 Hz. The continuous lines fitted through the scatter plots are impedance curves calculated using the circuit model shown in (c) for estimation of the film Rct. Within the circuit model, Rs is the solution resistance, Rdl is the double layer resistance, Rct is the film resistance, Cdl is the double layer capacitance, Q is the constant phase element of the film and W is the finite length Warburg impedance. The values for each element resulting from the modeling process are included in the Table S1 and S2. (d) Plots of ΔRct before and after exposing the TLR5 sensor to varying concentrations of *S. typhim*. (■) and *B. subtilis* (▲) ligands respectively. ΔRct = Rct (after immersion at a concentration) - Rct (before immersion). The EIS measurements were carried out in an electrochemical cell containing a 5 mM/5 mM $Fe(CN)_6^{3-/4-}$ aqueous solution with 1 M $NaClO_4$ as the supporting electrolyte.

In order to evaluate the electrochemical impedance signals triggered by different concentrations of the bacterial ligands, the TLR5 sensor surfaces were characterized before and after ligand exposure. As shown in Figure 4a, the curve sizes in the Nyquist plots increase following immersion of the TLR5 sensors in solutions of *S. typhim.*. Similar results are observed in parallel experiments conducted monitoring the signals triggered by concentrations of *B. subtilis* and this data is plotted in Figure 4b. The model shown in the Figure 4c was used to evaluate the film resistance (Rct) before and after each trial. The continuous lines in Figure 4a and b are from the modeling using ZSimpWin 2.0 and they are fit to the experimental curves. The calculated element values for the model are shown in the Table S1 and S2. The ΔRct for each concentration of the ligand was calculated by subtracting the Rct of the sensor before the ligand immersion from the total post-immersion Rct. The plots of ΔRct are illustrated in Figure 4d. After immersing the sensor in a 0.1 μM concentration of *S. typhim*. flagellins, a ΔRct of $526 \pm 10\ \Omega \cdot cm^2$ is observed. The ΔRct measured following sensor surface exposure to higher concentrations of *S. typhim*. flagellins is greater than that measured for lower concentration exposures. As expected, the ΔRct values measured for the sensor surface following immersion in each concentration of *B. subtilis* flagellins are consistently and proportionally smaller than for immersions in the same concentration series of *S. typhim*. flagellins, as shown in the Figure 4d. A statistical analysis was conducted using the ΔRct values obtained for each independent TLR5 ligand experiment, utilizing data collected for the entire concentration range; t-tests were conducted and p-values were obtained. As further detailed in Table S3, the statistical variance between the two data sets is significantly larger than the variance within the data points within each set. The p-values for 0.1 μM, 0.5 μM, 1 μM and 2 μM concentrations correspond to 2.7%, 1.1%, 3.8% and 2.0% respectively. These p-values are all below the 5% threshold. Therefore, the electrochemical responses corresponding to the detection of these two bacterial ligands at the same concentration are unlikely to be confused. This study reveals that the difference in molecular weights of the two ligand species possibly has a profound effect on the differentiation between their electrochemical signatures when examined under the same experimental conditions.

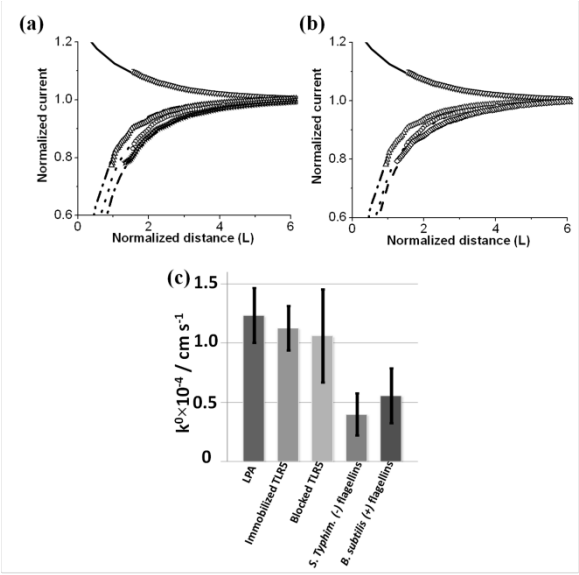

Figure 5. Examples of normalized SECM approach curves measured for the following surface assembly phases: (▽) bare gold; (△) gold modified with LPA; (○) immobilized TLR5 after ethanolamine blocking; (◇) after incubation with *S. typhim.* (-) flagellins (a); (☆) after incubation with *B. subtilis* (+) flagellins (b). The continuous and dashed lines are the approach curves calculated by COMSOL Multiphysics simulation using known values for the dimensionless rate constant (Λ). The current measured during the approach was normalized using the measured tip steady-state current at an infinite distance from the substrate. The normalized distance (L) is the ratio of the tip/substrate separation (d/a) to the tip radius. (c) Rate constant, k^0, plots for the surface following each modification step. These rate constants were calculated using the dimensionless rate constants Λ values estimated by the contrasting the experimental approach curve data against the calculated approach curve data shown in Figure 5a and b.

SECM has been chosen for the complementary investigation of the efficacy of the TLR5 sensor for the specific detection of its flagellin PAMPs. The working principle of SECM has been well reviewed in many publications and it is an extremely powerful detection technique for the exploration of bio-interactions.[41-44] The capacity of SECM for analytical detection has been demonstrated by Piotr *et al.* and Shamsi *et al.*.[35,36,45] In contrast to the three techniques described above, SECM allows the examination of localized film properties and was applied, within this study, for investigation of the same incremental surface architecture assembly procedure for the construction of a TLR5 sensor surface and the subsequent detection of the flagellin ligands. The SECM approach curves, shown in Figure 5a and b, demonstrate positive feedback on bare gold surfaces as expected due to its conductivity and fast electron transfer rate constant. As the Au surface was modified by LPA and TLR5 was immobilized, the approach curves reveal increasing negative feedback with each additional SAM layer. As expected, this demonstrates a dampening in the rate of electron transfer with each step of the sensor assembly. COMSOL modeling processes, using an RG5 tip, were carried out as described in previous publications [36,45] and the resulting curve simulations were used to evaluate the regeneration kinetics and electron transfer rates at the surface interface. A selection of these simulated approach curves are depicted in Figures S2a and b as represented by the continuous and dashed lines fitted under the collected raw data points. The charge transfer rate for each sensor modification step was evaluated and plotted in Figure 5c. The trend of the k^0 is in agreement with Rct shown in Figure S1c. The larger the Rct is, the slower k^0. Following independent exposures of the fabricated TLR5 sensors to the flagellins of *S. typhim.* and *B. subtilis* respectively, the k^0 determined is reduced further from 10.6 ± 3.9 cm•s^{-1} to 4.0 ± 1.8 cm•s^{-1} and 5.6 ± 2.3 cm•s^{-1}. The signals triggered by the two different ligand species cannot be differentiated using this detection method measurement, that being said, SECM is still capable of monitoring the surface changes triggered by each ligand species post-sensor exposure as compared to the results collected prior to ligand application. It is speculated that there is a larger relative error-to-signal ratio in SECM measurements as compared to that for EIS as a result of respective local and surface averaged characteristics of two techniques. The modification and immobilization measurements carried out at the surface on a microscale be more homogeneous than on macroscale. Nevertheless, the results from these different techniques are complementary to each other and provide a good foundation for the future development of these types of TLR sensors.

Conclusions

In conclusion, we have developed a biosensor that exploits TLR5 as a bio-recognition element for bacterial flagellins. The electrochemical properties of the incremental surface architecture assembly steps were probed using a combination of complementary techniques including CV, EIS and SECM. The results produced through the exploitation of these different electrochemical detection approaches are consistent with each other. Following its assembly, the sensor was challenged by applying solutions of flagellins, the TLR5 PAMP, from either Gram(-) (*S. typhim.)* or Gram(+) (*B. subtilis*) bacteria strains and the resulting binding response was examined. Depending on the molecular weight of the PAMP ligand and their electrochemical properties, responses varied and were quantitatively estimated by EIS approaches and supported by SWV and SECM. The study presented in this paper is the initial step toward a TLR5-based biosensor, which can be further developed and, subsequently, calibrated. The TLR5 receptor is only one member among those in the toll-like receptor suite; adapting the sensor architecture to exploit the unique recognition abilities of each TLR offers new opportunities for broad-spectrum pathogen diagnostics in near-real time. This initial investigation is an important milestone toward TLR-based detection assays.

ASSOCIATED CONTENT

Supporting Information

The experimental reagents and processes for electrode cleaning and preparation of TLR5 sensors are described in the supporting information. Supporting Information Available: This material is available free of charge via the Internet at http://pubs.acs.org.

AUTHOR INFORMATION

Corresponding Author

* Email: bkraatz@utsc.utoronto.ca. Tel: +1-416-287-7197. Fax: +1-416-287-7204.

Present Addresses

† Department of Chemistry, Beijing Institute of Technology, Beijing 100081, P. R. China.

Author Contributions

All authors have given approval to the final version of the manuscript. ‡These authors contributed equally.

ACKNOWLEDGMENT

We acknowledge Prof. Z. Ding (University of Western Ontario) for useful discussions on SECM and COMSOL experiments. The funding provided by Defence R&D Canada through a competitive contract "EIS Detection of Biological Agents" is greatly appreciated. The period of the contract is from October 11, 2012 to March 31, 2014 inclusive.

REFERENCES

(1) Merkl, S.; Vornicescu, D.; Dassinger, N.; Keusgen, M. *Phys. Status Solidi A* **2014**, *211*, 1416.
(2) Heyduk, E.; Heyduk, T. *Analytical Biochemistry* **2010**, *396*, 298.
(3) Guo, X.; Lin, C.-S.; Chen, S.-H.; Ye, R.; Wu, V. C. H. *Biosensors & Bioelectronics* **2012**, *38*, 177.
(4) Wangmaung, N.; Chomean, S.; Promptmas, C.; Mas-oodi, S.; Tanyong, D.; Ittarat, W. *Biosens. Bioelectron.* **2014**, *62*, 295.
(5) Lu, L.; Chee, G.; Yamada, K.; Jun, S. *Biosensors & Bioelectronics* **2013**, *42*, 492.
(6) Barreiros dos Santos, M.; Agusil, J. P.; Prieto-Simon, B.; Sporer, C.; Teixeira, V.; Samitier, J. *Biosensors & Bioelectronics* **2013**, *45*, 174.
(7) Maalouf, R.; Fournier-Wirth, C.; Coste, J.; Chebib, H.; Saikali, Y.; Vittori, O.; Errachid, A.; Cloarec, J.-P.; Martelet, C.; Jaffrezic-Renault, N. *Analytical Chemistry* **2007**, *79*, 4879.
(8) Nadkarni, M. A.; Martin, F. E.; Jacques, N. A.; Hunter, N. *Microbiology (Reading, U. K.)* **2002**, *148*, 257.
(9) Baccar, H.; Mejri, M. B.; Hafaiedh, I.; Ktari, T.; Aouni, M.; Abdelghani, A. *Talanta* **2010**, *82*, 810.
(10) Li, Y.; Afrasiabi, R.; Fathi, F.; Wang, N.; Xiang, C.; Love, R.; She, Z.; Kraatz, H.-B. *Biosensors and Bioelectronics* **2014**, *58*, 193.
(11) Mannoor, M. S.; Zhang, S.; Link, A. J.; McAlpine, M. C. *Proceedings of the National Academy of Sciences of the United States of America* **2010**, *107*, 19207.
(12) Yang, L.; Ruan, C.; Li, Y. *Biosens. Bioelectron.* **2003**, *19*, 495.
(13) Yang, L.; Bashir, R. *Biotechnol. Adv.* **2008**, *26*, 135.
(14) Yang, L. *Talanta* **2008**, *74*, 1621.
(15) Barlaan, E. A.; Sugimori, M.; Furukawa, S.; Takeuchi, K. *J. Biotechnol.* **2005**, *115*, 11.
(16) Ikeda, M.; Yamaguchi, N.; Tani, K.; Nasu, M. *J. Health Sci.* **2006**, *52*, 36.
(17) Britschgi, T. B.; Cangelosi, G. A. *Mol. Cell. Probes* **1995**, *9*, 19.
(18) Liu, R. H.; Yang, J.; Lenigk, R.; Bonanno, J.; Grodzinski, P. *Anal. Chem.* **2004**, *76*, 1824.
(19) Ligaj, M.; Tichoniuk, M.; Gwiazdowska, D.; Filipiak, M. *Electrochim. Acta* **2013**, Ahead of Print.
(20) Luo, C.; Tang, H.; Cheng, W.; Yan, L.; Zhang, D.; Ju, H.; Ding, S. *Biosens. Bioelectron.* **2013**, *48*, 132.
(21) Jiang, D.; Xiang, G.; Wu, J.; Liu, C.; Liu, F.; Pu, X. *Int. J. Electrochem. Sci.* **2012**, *7*, 5273.
(22) Ivnitski, D.; Abdel-Hamid, I.; Atanasov, P.; Wilkins, E.; Stricker, S. *Electroanalysis* **2000**, *12*, 317.
(23) Liao, J. C.; Mastali, M.; Li, Y.; Gau, V.; Suchard, M. A.; Babbitt, J.; Gornbein, J.; Landaw, E. M.; McCabe, E. R. B.; Churchill, B. M.; Haake, D. A. *J. Mol. Diagn.* **2007**, *9*, 158.
(24) Uzarski, J. R.; Mello, C. M. *Anal. Chem. (Washington, DC, U. S.)* **2012**, *84*, 7359.
(25) da Silva, J. S. L.; Oliveira, M. D. L.; de Melo, C. P.; Andrade, C. A. S. *Colloids Surf., B* **2014**, Ahead of Print.
(26) Abdul Rahman, M. S.; Mukhopadhyay, S. C.; Yu, P.-L.; Goicoechea, J.; Matias, I. R.; Gooneratne, C. P.; Kosel, J. *J. Food Eng.* **2013**, *114*, 346.
(27) Lei, W.; Jiang, G.; Zhou, Q.; Hou, Y.; Zhang, B.; Cheng, X.; Wang, X. *Sens. Actuators, B* **2012**, *166-167*, 853.
(28) Janeway, C. A., Jr.; Medzhitov, R. *Annu. Rev. Immunol.* **2002**, *20*, 197.
(29) Kang, J. Y.; Lee, J. O. In *Annual Review of Biochemistry, Vol 80*; Kornberg, R. D., Raetz, C. R. H., Rothman, J. E., Thorner, J. W., Eds. 2011; Vol. 80, p 917.
(30) Jin, M. S.; Lee, J. O. *Immunity* **2008**, *29*, 182.
(31) Mogensen, T. H. *Clin. Microbiol. Rev.* **2009**, *22*, 240.
(32) Olguin, Y.; Villalobos, P.; Carrascosa, L. G.; Young, M.; Valdez, E.; Lechuga, L.; Galindo, R. *Analytical and Bioanalytical Chemistry* **2013**, *405*, 1267.
(33) Hayashi, F.; Smith, K. D.; Ozinsky, A.; Hawn, T. R.; Yi, E. C.; Goodlett, D. R.; Eng, J. K.; Aidra, S.; Underhill, D. M.; Aderem, A. *Nature (London, U. K.)* **2001**, *410*, 1099.
(34) Chornokur, G.; Arya, S. K.; Phelan, C.; Tanner, R.; Bhansali, S. *J. Sens.* **2011**, 983752.
(35) Shamsi, M. H.; Kraatz, H. B. *Analyst* **2011**, *136*, 4724.
(36) Alam, M. N.; Shamsi, M. H.; Kraatz, H. B. *Analyst* **2012**, *137*, 4220.
(37) Diakowski, P. M.; Kraatz, H.-B. *Chemical Communications* **2009**, 1189.
(38) Tanious, F. A.; Nguyen, B.; Wilson, W. D. *Methods Cell Biol* **2008**, *84*, 53.
(39) Martic, S.; Beheshti, S.; Kraatz, H. B.; Litchfield, D. W. *Chemistry & Biodiversity* **2012**, *9*, 1693.
(40) Labib, M.; Shipman, P. O.; Martic, S.; Kraatz, H. B. *Analyst* **2011**, *136*, 708.
(41) Kwak, J.; Bard, A. J. *Analytical Chemistry* **1989**, *61*, 1221.
(42) Mirkin, M. V.; Fan, F. R. F.; Bard, A. J. *J. Electroanal. Chem.* **1992**, *328*, 47.
(43) Amphlett, J. L.; Denuault, G. *J. Phys. Chem. B* **1998**, *102*, 9946.
(44) Bergner, S.; Vatsyayan, P.; Matysik, F.-M. *Anal. Chim. Acta* **2013**, *775*, 1.
(45) Diakowski, P. M.; Kraatz, H. B. *Chemical Communications* **2011**, *47*, 1431.

For TOC only